Polymer Journal (2019) 51:1045–1053
https://doi.org/10.1038/s41428-019-0212-5

ORIGINAL ARTICLE

Water-induced surface reorganization of bioscaffolds composed of an amphiphilic hyperbranched polymer

Hisao Matsuno[1,2] · Masayasu Totani[1] · Arisa Yamamoto[3] · Masayuki Haraguchi[4] · Masaaki Ozawa[4] · Keiji Tanaka[1,2,3]

Received: 14 April 2019 / Revised: 4 May 2019 / Accepted: 7 May 2019 / Published online: 11 June 2019

Abstract

The ability to freely control the surface of bioscaffolds in a water environment is desirable to regulate cellular behaviors in vitro. Herein, we study the surface aggregation states of scaffold films composed of a multifunctional hyperbranched polymer (HBP) with perfluorohexylethyl, carboxy, and cyano groups that was prepared using a spin-coating method. Static contact angle measurements in conjunction with X-ray photoelectron spectroscopy revealed that perfluorohexylethyl groups were segregated at the surface of the HBP film in air, and these findings were more remarkable for the film treated with thermal annealing. Once the HBP film contacted water, HBP chains reorganized at the surface to minimize the free energy, resulting in the formation of a relatively hydrophilic surface. This surface reorganization was discernably faster and more remarkable for the non-annealed HBP film than for the annealed film. As fundamental characteristics of a cellular scaffold, protein adsorption, in addition to the initial adhesion and proliferation of fibroblasts, was examined using microscopy. The amount of fibronectin adsorbed depended on the presence of thermal annealing during the scaffold preparation process. A relatively larger amount of fibronectin adsorbed to the non-annealed HBP film promoted the initial adhesion and subsequent proliferation of fibroblasts.

Introduction

One of the strategies for assisting in the evolution of biotechnology and regenerative medicine is the investigation of bioscaffolds. Numerous types of polymeric scaffolds have been developed based on various chemical and physical processes to control the interaction between scaffold surfaces and biological substances in vitro [1–3]. In addition, researchers have extensively studied how and why polymer characteristics affect protein adsorption and cellular behaviors such as adhesion, proliferation, migration, and differentiation [4–21]. These investigations have led to the established hypothesis that various surface factors, such as the chemical composition [5–7], free energy [5–7, 9], crystallinity [10, 11], topology [12–14], and mechanical properties [5, 8, 15–21], are keys regulating cellular functions in culture systems in vitro.

These bioscaffolds are used in water environments. Thus, a better understanding of the aggregation states and physical properties of polymer chains in the outermost region of the scaffolds in water is needed as a first benchmark. In general, however, these properties are highly dependent on the contacting medium [22–27], which affects their functional performance [25–27], because the aggregation states of chains in the outermost region are reorganized to minimize the free energy at the interface. In addition, polymer segments in the interfacial region might be partially dissolved by/swollen in water, depending on the interaction between

✉ Hisao Matsuno
h-matsuno@cstf.kyushu-u.ac.jp

✉ Keiji Tanaka
k-tanaka@cstf.kyushu-u.ac.jp

[1] Department of Applied Chemistry, Kyushu University, Fukuoka 819-0395, Japan

[2] International Institute for Carbon-Neutral Energy Research (WPI-I2CNER), Kyushu University, Fukuoka 819-0395, Japan

[3] Department of Automotive Science, Kyushu University, Fukuoka 819-0395, Japan

[4] Materials Research Laboratories, Nissan Chemical Corporation, Chiba 274-0052, Japan

segments and water. These changes have been observed for poly(methyl methacrylate) (PMMA) in water [22].

Here, we focus on a hyperbranched polymer (HBP) [28–33] in a thin film state [34–36] as a cellular scaffold. HBP is regarded as a polymer in between a conventional linear and a well-defined dendritic macromolecule. It is prepared through a simple procedure using a one-pot reaction, unlike the stepwise synthesis required for dendrimers, with essentially no further purification. One of the advantages of HBP is the particularly large number of terminal groups per molecule that are easily chemically modified [37, 38]. Thus, based on this unique architecture, HBP has attracted increasing attention in material science. In particular, biodegradable [39, 40] and porous hydrogel [41, 42] HBP scaffolds have been reported. However, despite the growing body of literature on HBP-containing scaffolds for cell culture, less is known about the relationship between the aggregation states of the HBP surface and cellular behaviors.

The purpose of this study is to obtain a better understanding of the water-induced surface reorganization of an HBP scaffold containing hydrophobic and hydrophilic groups and to discuss how it affects the biological events on it.

Experimental procedures

Preparation of HBP films

HBP with a number-average molecular weight (M_n) of 7.4k and an M_w/M_n of 4.0, where M_w is the weight-average molecular weight, was obtained from Nissan Chemical Corp. (Tokyo, Japan). Figure 1 shows the chemical structure of HBP. The molar ratio of divinyl benzene unit/2-perfluorohexylethyl acrylate unit/chain-end carboxy group in HBP was determined to be 1.00/0.59/0.99 based on ^{1}H- and ^{13}C-nuclear magnetic resonance spectroscopy using an ECZ-400S spectrometer (JEOL, Ltd., Tokyo, Japan). The glass transition temperature (T_g) of HBP was determined to be 338 K using differential scanning calorimetry (EXSTAR6000 DSC6220, Hitachi High-Tech Science, Corp., Tokyo, Japan). Thin films of HBP were prepared on various solid substrates such as a Si-wafer and a borosilicate glass using a spin-coating method from a tetrahydrofuran solution. The thickness of the films was approximately 170 nm. The HBP films were dried at room temperature or annealed at 358 K, which was 20 K higher than the T_g, under vacuum for 24 h. Hereafter, the former and latter films are referred to as 'non-annealed' and 'annealed' HBP films, respectively.

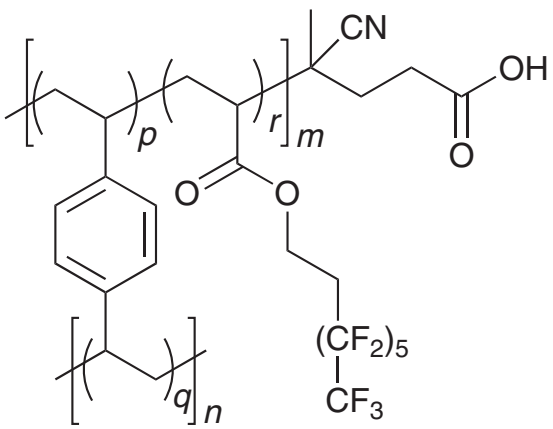

Fig. 1 Chemical structure of the divinyl benzene-based HBP-containing perfluorohexylethyl, carboxy, and cyano groups

Surface characterization of HBP films

The surface morphology of non-annealed and annealed HPB films on Si-wafers was observed using atomic force microscopy (AFM, E-sweep, Hitachi High-Tech Science, Corp., Tokyo, Japan) in dynamic force mode at room temperature under ambient conditions. A cantilever with a nominal spring constant of 1.3 N m^{-1} was used and the driving frequency was set to 27 kHz. The wettability of the HBP films was examined by recording static and dynamic contact angles at room temperature using a Drop Master 500 (Kyowa Interface Science, Co., Ltd., Saitama, Japan). A droplet of ultrapure water, which was purified using a Milli-Q system (Merck KGaA, Darmstadt, Germany), and diiodomethane were used as a probe. For static contact angle measurements, the volume of each probe was set to 1 μL and the values were recorded 1 s after each droplet contacted the film surfaces. A tilting cradle was used for dynamic contact angle measurements. An HBP film on a Si-wafer was tilted until the water droplet with a volume of 90 μL started to slide down it, and then the advancing (θ_a), receding (θ_r), and the roll-off or sliding angles (α) were recorded. In addition, static contact angles of an air bubble (θ_{air}) with a volume of 2 μL against the HBP films in water were also tracked over time. The data were recorded from 1 min to 24 h after immersion. The surface chemical composition of the HBP films was examined with angular dependent X-ray photoelectron spectroscopy (AD-XPS) using an APEX instrument (ULVAC-PHI, Kanagawa, Japan) at 2.0×10^{-7} Pa using a monochromatic Al-K_α X-ray source at 100 W. The emission angle (φ_e) of photoelectrons ranged from 15 to 90°. A C_{1s} peak was calibrated to a binding energy of 285.0 eV for a neutral carbon to correct the charging energy shifts.

Bioassays on HBP films

The amounts of proteins the adsorbed to the HPB films on borosilicate glass were examined using a BZ-8100

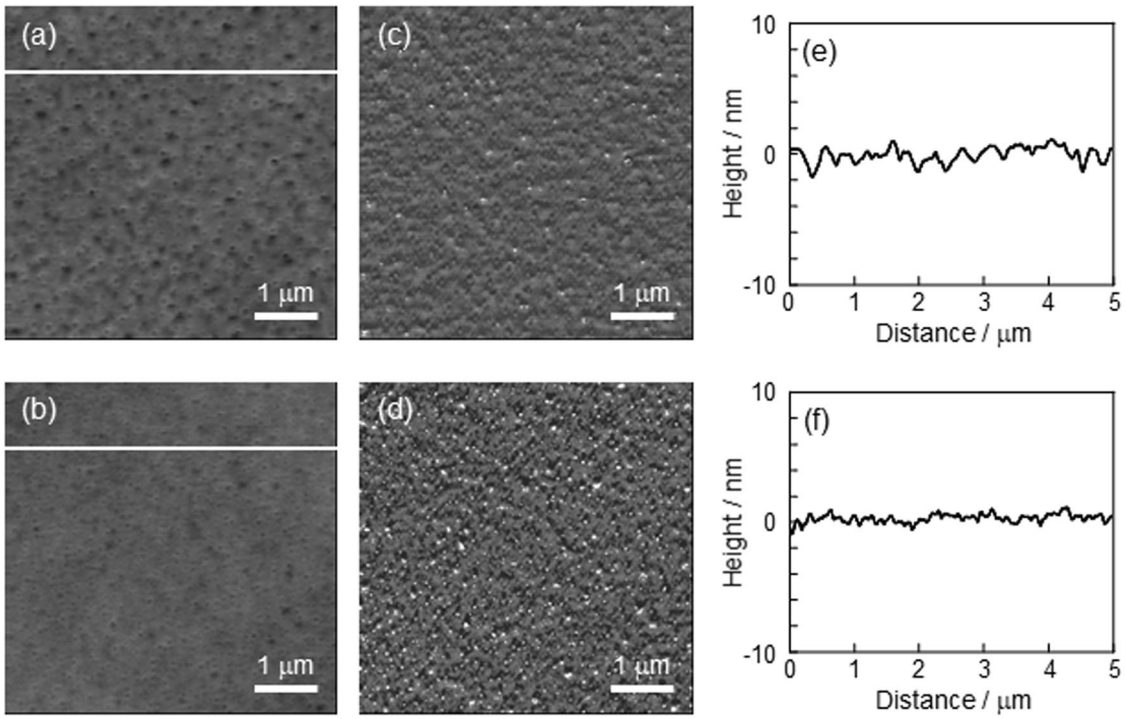

Fig. 2 AFM height (**a**, **b**) and phase images (**c**, **d**) of HBP films. (**e**, **f**) Sectional views along a line in (**a**, **b**). Panels **a**, **c**, **e**, and **b**, **d**, **f** show non-annealed and annealed films, respectively

fluorescence microscope (KEYENCE, Corp., Osaka, Japan). Fluorescein isothiocyanate-labeled bovine serum albumin (FITC-BSA, Elastin Products Company, Inc., Owensville, MO, USA) and rhodamine-conjugated fibronectin (Rho-FN, Cytoskeleton, Inc., Denver, CO, USA) were used as model proteins. Prior to the test, the HBP films were immersed in ultrapure water for 24 h and subsequently immersed in a 20 μg mL^{-1} solution of each protein in phosphate-buffered saline (PBS) for 1 h at 310 K (37 °C). The film surface was rinsed with PBS three times, and then the fluorescence intensity of proteins attached to the surface was recorded in PBS. The excitation/emission wavelengths were 494/520 nm and 535/585 nm for FITC-BSA and Rho-FN, respectively.

The adhesion and proliferation of mouse L929 fibroblasts (RIKEN BRC Cell Bank, Tsukuba, Japan) on the HBP films were examined under serum-free and 10% fetal bovine serum (FBS) conditions. The HBP films were placed at the base of a 24-well culture dish filled with ultrapure water for 24 h. Afterwards, ultrapure water was substituted with normal Roswell Park Memorial Institute 1640 culture media (Thermo Fisher Scientific, Inc., Waltham, MA, USA) supplemented with or without 10% FBS and then incubated for 1 h. L929 cell suspensions were seeded into the plate at a density of 5.0×10^4 cells/well. Cultures were maintained at 310 K under a 5% CO_2 atmosphere. Adhesion and proliferation were observed using phase-contrast microscopy. The quantitative data are presented as means ± standard deviations (SD). Statistical analysis was performed by Student's *t*-test.

Results and discussion

Surface aggregation states

First, the surface morphology of non-annealed and annealed HBP films was observed. Figure 2 shows AFM height (a and b) and phase images (c and d) of non-annealed (a and c) and annealed (b and d) HBP films in air. The root-mean-square roughnesses of the non-annealed and annealed films were 0.55 and 0.37 nm, respectively, and the films were sufficiently flat for further characterization.

Next, the static contact angle of liquid probes against the HBP films was examined to determine their wettability. Table 1 summarizes the data. While the static contact angle values of water (θ_w) against both HBP films were approximately the same, regardless of the thermal annealing, the static contact angle of diiodomethane (θ_d) against the annealed film was greater than the non-annealed film. Consequently, the surface free energy (γ_s) estimated using Owens' procedure was lower for the annealed HBP film than for the non-annealed film. These γ_s values were much lower than polystyrene (PS, ~40 mJ m^{-2}) [43], which has a similar chemical structure to HBP, and comparable to the values for fluorinated poly(methacrylate) derivatives,

Table 1 Static contact angle values of water (θ_w) and diiodomethane (θ_d) against non-annealed and annealed HBP films and their surface free energies (γ_s)

Film	θ_w/°	θ_d/°	γ_s/mJ m^{-2}
Non-annealed	109.5 ± 2.0	91.5 ± 1.5	12.5
Annealed	110.3 ± 1.1	98.4 ± 1.6	10.2

ranging from 10 to 20 mJ m^{-2} [43]. Thus, the HBP film surface was considerably hydrophobic. A probable explanation for this finding is that the hydrophobic perfluorohexyl groups in HBP were segregated at the outermost region of the film due to its lower free energy. The extent of this segregation was therefore predicted to be more remarkable after the thermal annealing condition.

XPS measurements were recorded to confirm this hypothesis. Figure 3 shows F_{1s} (a), O_{1s} (b) and C_{1s} (c and d) core-level spectra for the non-annealed and annealed HBP films on Si-wafers acquired at φ_e of 15°, which corresponds to an analytical depth of approximately 3 nm. Both HBP films showed a single peak in the F_{1s} spectra, indicating that fluorinated side chains were located in the outermost region of the films. The O_{1s} spectra showed two components at ~532 and 534 eV that corresponded to O*–C and O* = C, respectively. The intensity ratios of carbonyl oxygen to all O_{1s} ($I_{O=C}/I_{O1s}$) were 0.65 and 0.53, respectively, for the non-annealed and annealed films. In the C_{1s} region, four clear peaks and one shoulder were observed for both films. Signals at approximately 285.0, 286.5, 289.4, 291.8, and 294.5 eV were assigned to C-C*-C, C*-O or C*≡N, C* = O or C*-CF_2, C*-F_2, and C*-F_3, respectively [38, 44]. The intensity of the peaks from difluoromethylene (I_{CF2}) and trifluoromethyl (I_{CF3}) carbons seemed to be slightly stronger for the annealed film than for the non-annealed film.

Figure 3e shows the XPS intensity ratio of fluorinated carbons to all carbons, namely, $(I_{C^*-F2} + I_{C^*-F3})/I_{C1s}$, as a function of sin φ_e. The bulk value (0.16) calculated based on the chemical structure of HBP is also shown as a blue dashed line. All experimental values were greater than bulk values, even at the deepest depth probed. The intensity ratio increased with decreasing sin φ_e for both films. Based on these findings, perfluorohexyl groups were segregated at the film surface. The dotted and solid curves shown in Fig. 3e are the best-fit curves to the experimental data based on the model depth profiles shown in Fig. 3f. The extent of the segregation became more remarkable after the annealing treatment. This finding is very consistent with the results of the contact angle measurements.

Water-induced surface reorganization

In general, polymer segments in a film segregate at an interface to minimize the interfacial free energy in response to a change in the surrounding environment. We therefore subsequently examined the surface reorganization of the non-annealed and annealed HBP films as they contacted water. Table 2 summarizes the dynamic contact angles of a water droplet against the HBP films. The data clearly depended on the annealing process. The contact angle hysteresis ($\Delta\theta$) was simply defined as θ_a–θ_r. The $\Delta\theta$ value for the non-annealed film was approximately 9° greater than for the annealed film, mainly due to the difference of θ_r, implying that surface segments were more mobile in the non-annealed film than in the annealed film. A probable explanation for this finding is that chains in the non-annealed film were not densely packed [23]. Then, surface reorganization, which was achieved by the migration of hydrophilic carboxy and cyano groups and hydrophobic fluoroalkyl groups to the outermost and inner regions, respectively, occurred. In addition, the α value, at which a water drop starts to roll off a tilted surface, was greater for the non-annealed film than for the annealed film.

Figure 4 shows the θ_{air} against the HBP films as a function of the water immersion time (t). Figure 4b is an enlarged plot only in the initial period. In addition, the ideal initial θ_{air} value ($\theta_{air}(t = 0)$), which is simply estimated by 180–θ_w, is also shown. The values were 70.5° and 69.7° for the non-annealed and annealed films, respectively. For both films, θ_{air} increased with an increasing time immersed in water, indicating that the outermost region of the film became more hydrophilic when in direct contact with water. The rate of increase in θ_{air} for the non-annealed film was greater than for the annealed film. The time required to reach a constant θ_{air} was ~0.5 and 6 h for the non-annealed and annealed films, respectively. Taking into account the expected $\theta_{air}(t = 0)$ values, a reasonable hypothesis is that chains in the outermost region in the HBP films started to rearrange immediately after contacting water. In a *quasi*-equilibrium state, the θ_{air} values reached 131.6° and 125.2° for the non-annealed and annealed films, respectively. These values correspond to increases in the θ_{air} value of 61.1° and 55.5°, respectively. As previously reported, an annealed PMMA film also becomes more hydrophilic due to a change in the local conformation as it contacts water. However, at that time point, the increase in θ_{air} is only ~6° [25]. Thus, we postulated that the water-induced reorganization of HBP chains in the outermost region of the film was quite remarkable compared with conventional homopolymers due to the presence of hydrophobic perfluorohexylethyl and hydrophilic carboxy and cyano groups.

Scaffold properties

Finally, the cellular scaffold properties of the surface-reorganized HBP films were characterized. Based on the θ_{air}

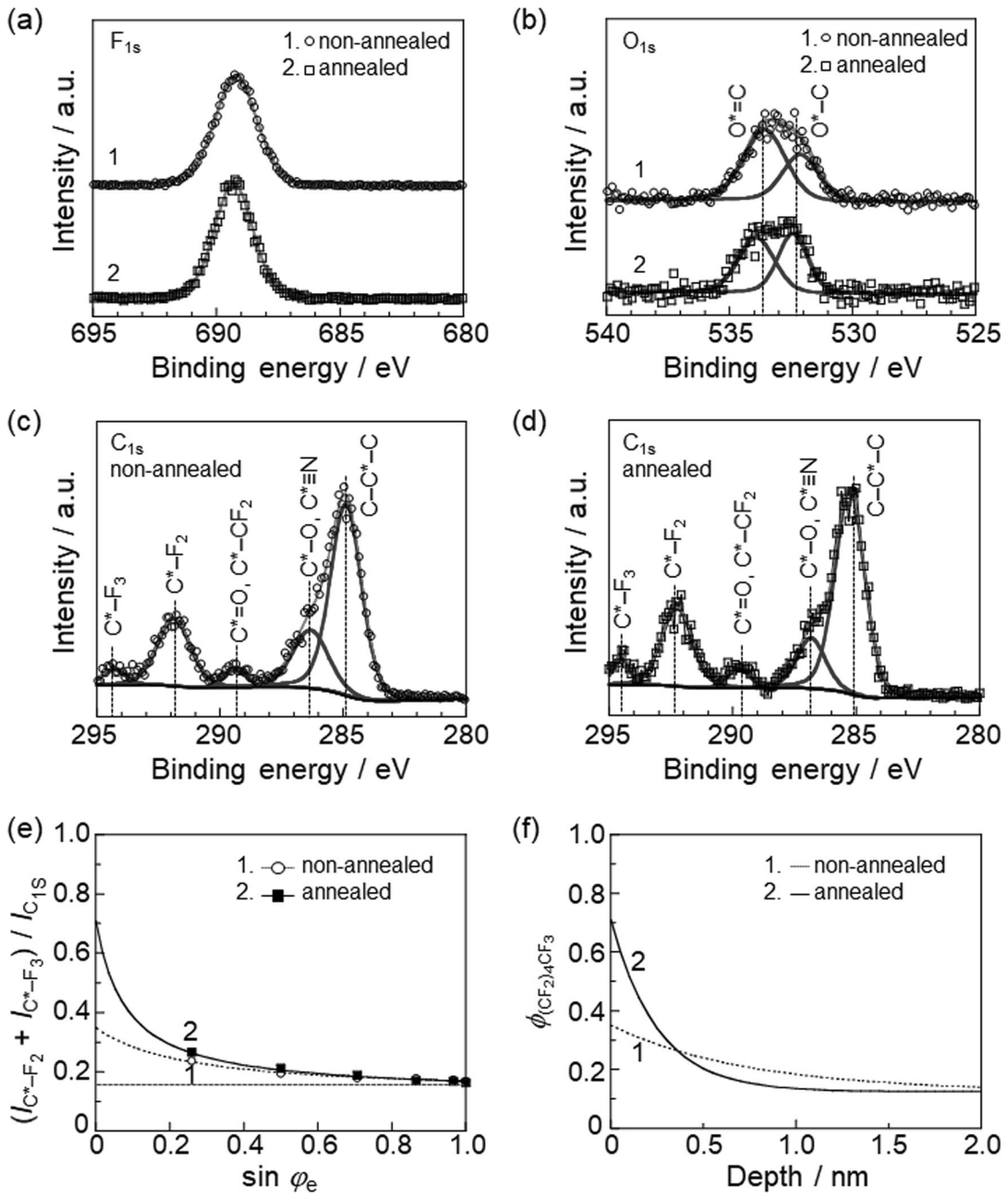

Fig. 3 F_{1s} (**a**), O_{1s} (**b**), and C_{1s} (**c**, **d**) core-level XPS spectra for non-annealed and annealed HBP films, respectively. Open symbols denote experimental signals. While both red and blue curves show the results of curve fitting, the red curve represents the summation of the blue curves. (**e**) Intensity ratio of fluorinated carbon species to all carbons ($(I_{C^*-F2} + I_{C^*-F3})/I_{C1s}$) as a function of sin φ_e. Dotted and solid curves in panel **e** are best fits to the experimental $(I_{C^*-F2} + I_{C^*-F3})/I_{C1s}$ vs. sin φ_e relation based on the model depth profiles shown in panel (**f**)

Table 2 Data for dynamic contact angle measurements for non-annealed and annealed HBP films

Film	θ_a/°	θ_r/°	$\Delta\theta$/°	α/°
Non-annealed	110.9 ± 3.0	36.6 ± 1.3	74.3 ± 1.7	57.3 ± 2.1
Annealed	112.4 ± 2.3	46.9 ± 0.5	65.5 ± 1.8	47.3 ± 1.5

measurements, all films were immersed in ultrapure water for 24 h to achieve a *quasi*-equilibrium state before the tests. Figure 5 shows fluorescence microscopy images of Rho-FN (a and b) and FITC-BSA (c and d) adsorbed to the non-annealed (a and c) and annealed (b and d) HBP films. Both Rho-FN and FITC-BSA were uniformly adsorbed onto the HBP films. The amount of proteins adsorbed depended on the presence of the

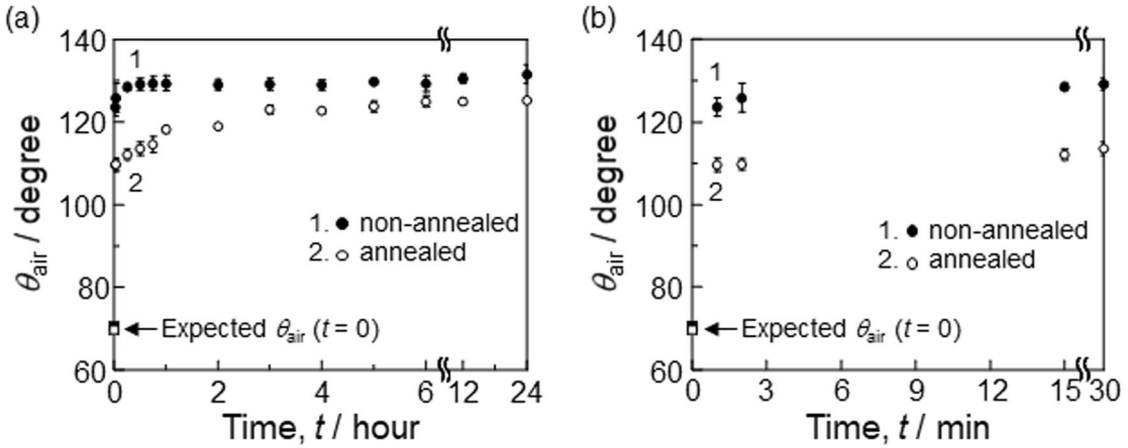

Fig. 4 (**a**) Immersion time dependence of the static contact angle of an air bubble (θ_{air}) against non-annealed and annealed HBP films. (**b**) An enlarged view of the initial stage shown in panel **a**. Expected θ_{air} values at $t = 0$ are also depicted as closed and open squares for non-annealed and annealed HBP films, respectively

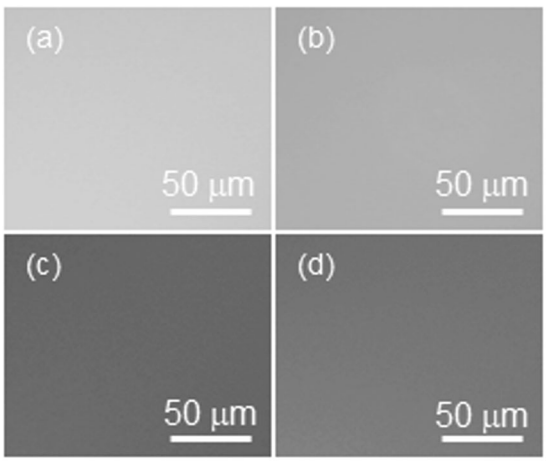

Fig. 5 Fluorescence microscopy images of Rho-FN (**a**, **b**) and FITC-BSA (**c**, **d**) adsorbed on non-annealed (**a**, **c**) and annealed (**b**, **d**) HBP films

annealing treatment. The adsorption of Rho-FN and FITC-BSA was more and less remarkable, respectively. We postulate that fibronectin plays a role as an extracellular matrix (ECM) protein in enhancing successive cell adhesion and proliferation [45], and thus cells cultured on the non-annealed HBP film should become more active because a greater amount of fibronectin was adsorbed on the film.

The behaviors of cells cultured on the HBP films were examined to confirm this hypothesis. Before cell culture under a standard serum condition (10% FBS), cell adhesion was analyzed under a serum-free condition to evaluate the toxicity of the HBP films. Figure 6a–c show phase-contrast microscopy images of L929 fibroblasts attached to each film after culture under serum-free conditions for 4 h. As a reference, the data for a commercially available tissue culture polystyrene (TCPS) dish are also shown [46–48]. While cells attached to all the surfaces, the number (N_{L929}) and the morphology of adherent L929 fibroblasts depended on each surface. Although the N_{L929} value for the non-annealed HBP film was comparable to TCPS, it decreased for the annealed film, as shown in Fig. 6d. Therefore, the non-annealed HBP film was not toxic to L929 fibroblasts at the very least.

The cell culture was then conducted in the presence of serum. Figure 7 shows the culture time-dependent growth of N_{L929} (growth curves). During both the initial adhesion process evaluated after 4 h of culture and proliferation processes from 4 h to 3 days of culture, the N_{L929} value was greater for the non-annealed film than that for the annealed film. Generally, fibronectin present in serum adsorbs quickly on a culture substrate before cell attachment. Based on the result that a greater amount of fibronectin adsorbed to the non-annealed film than to the annealed film, as discussed above, a reasonable hypothesis is that more cells proliferated on the non-annealed film than on the annealed film. In addition, the growth curve for the non-annealed film was comparable to TCPS. Thus, because the surface of TCPS was prepared using a plasma treatment, the surface design using HBP has advantages of the wide applicability to devices with a complicated shape, such as three dimensional microchannels [48, 49], in addition to the processing cost.

Conclusions

Aggregation states at the surface of spin-coated films composed of a multifunctional HBP were examined in air and aqueous environments by measuring the contact angle and XPS and recording AFM observations. The HBP film formed a somewhat hydrophobic surface under an

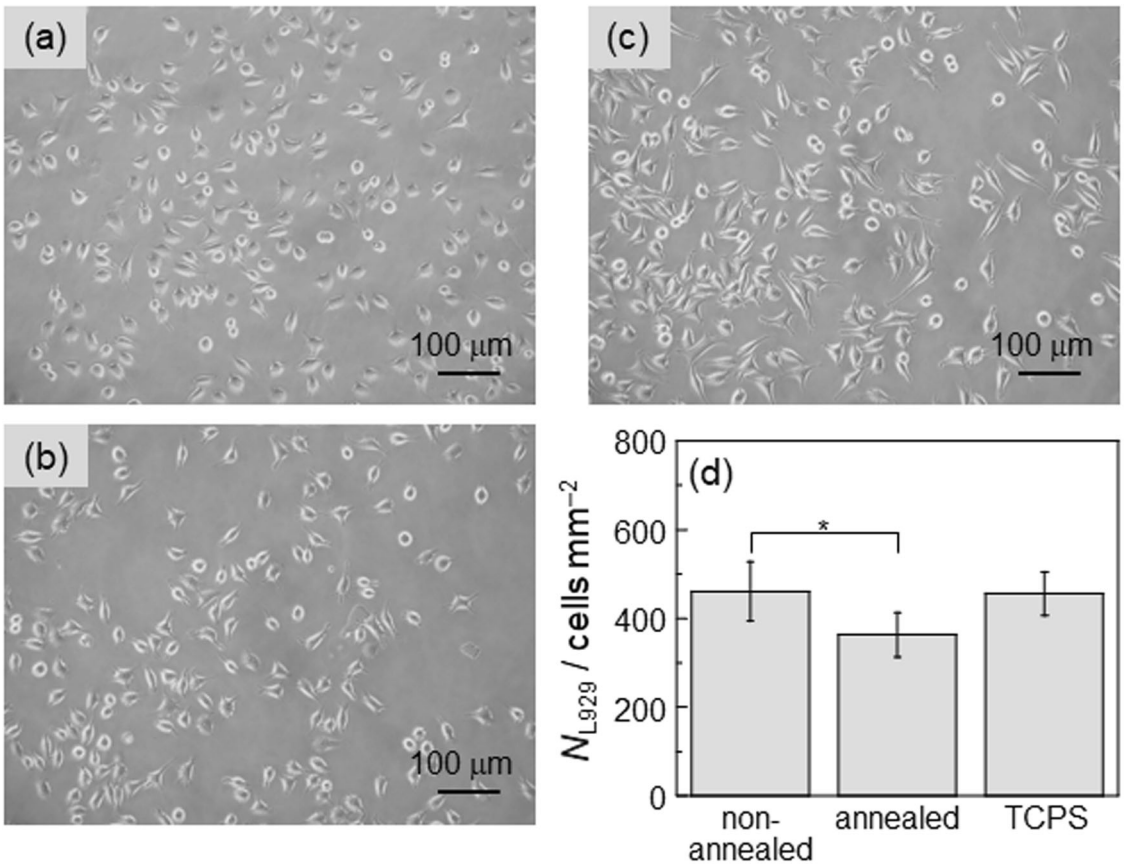

Fig. 6 Phase-contrast images of L929 fibroblasts adhered on (**a**) non-annealed and (**b**) annealed HBP films, and (**c**) TCPS after culture under serum-free conditions for 4 h. (**d**) Number of cells (N_{L929}) that adhered to each film. Data are presented as means ± SD. *$P < 0.05$ (Student's *t*-test)

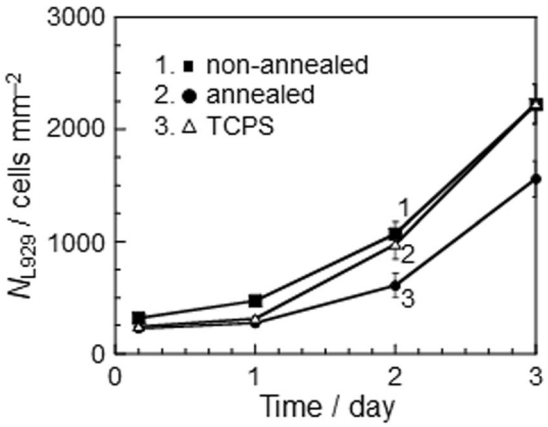

Fig. 7 Growth curves of L929 fibroblasts cultured on non-annealed and annealed HBP films, and a reference, TCPS. Data are presented as means ± SD

ambient condition due to the segregation of perfluorohexylethyl groups. However, the surface became hydrophilic when the film contacted water. The extent of the surface reorganization became less remarkable once the film was thermally annealed. An explanation for these findings is the loose or dense packing state of HBP chains in the film before and after annealing. Fibronectin was well adsorbed on the surface of the non-annealed film and promoted cell adhesion and proliferation. The multifunctional HBP used here can be further modified with functional molecules. We propose that the non-annealed HBP film has great potential as a bioscaffold for in vitro cell culture systems.

Acknowledgements We are grateful to Nissan Chemical Corp. for kindly providing HBP. This research was partially supported by a JSPS KAKENHI Grant-in-Aid for Scientific Research (A) (Grant No. JP15H02183) (K.T.), Grant-in-Aid for Scientific Research (B) (Grant No. JP18H02037) (H.M.), and Early-Career Scientists (Grant No. JP18K16990) (M.T.). We are also grateful for support from JST-Mirai Program (JPMJMI18A2) and CSTI Impulsing Paradigm Change through Disruptive Technologies (ImPACT) Program (K.T.).

Compliance with ethical standards

Conflict of interest The authors declare that they have no conflict of interest.

References

1. Shastri VP, Lendlein A. Materials in regenerative medicine. Adv Mater. 2009;21:3231–4.
2. Xu W, Wang Z, Li T, Wang L, Zhang W, Liang Y, et al. Membranes based on carboxymethyl chitin as potential scaffolds for corneal endothelial transplantation. Polym J. 2017;49:789–98.
3. Kambe Y, Tokushige T, Mahara A, Iwasaki Y, Yamaoka T. Cardiac differentiation of induced pluripotent stem cells on elastin-like protein-based hydrogels presenting a single-cell adhesion sequence. Polym J. 2019;51:97–105.
4. Ratner BD, Bryant SJ. Biomaterials: where we have been and where we are going. Annu Rev Biomed Eng. 2004;6:41–75.
5. Alves NM, Pashkuleva I, Reis RL, Mano JF. Controlling cell behavior through the design of polymer surfaces. Small. 2010;6: 2208–20.
6. Yao X, Peng R, Ding J. Cell-material Interactions revealed via material techniques of surface patterning. Adv Mater. 2013;25: 5257–86.
7. Tamada Y, Ikada Y. Fibroblast growth on polymer surfaces and biosynthesis of collagen. J Biomed Mater Res. 1994;28:783–9.
8. Benoit DSW, Schwartz MP, Durney AR, Anseth KS. Small functional groups for controlled differentiation of hydrogel-encapsulated human mesenchymal stem cells. Nat Mater. 2008;7:816–823.
9. Gentleman MM, Gentleman E. The role of surface free energy in osteoblast–biomaterial interactions. Int Mater Rev. 2014;59: 417–29.
10. Park A, Cima LG. *In vitro* cell response to differences in poly-L-lactide crystallinity. J Biomed Mater Res. 1996;31:117–30.
11. Simon CG Jr., Eidelman N, Kennedy SB, Sehgal A, Khatri CA, Washburn NR. Combinatorial screening of cell proliferation on poly(L-lactic acid)/poly(D,L-lactic acid) blends. Biomaterials. 2005;26:6906–15.
12. Dalby MJ, Gadegaard N, Tare R, Andar A, Riehle MO, Herzyk P, et al. The control of human mesenchymal cell differentiation using nanoscale symmetry and disorder. Nat Mater. 2007;6:997–1003.
13. Greco F, Fujie T, Ricotti L, Taccola S, Mazzolai B, Mattoli V. Microwrinkled conducting polymer interface for anisotropic multicellular alignment. ACS Appl Mater Interfaces. 2013;5: 573–84.
14. Viswanathan P, Ondeck MG, Chirasatitsin S, Ngamkham K, Reilly GC, Engler AJ, et al. 3D surface topology guides stem cell adhesion and differentiation. Biomaterials. 2015;52:140–7.
15. Discher DE, Janmey P, Wang YL. Tissue cells feel and respond to the stiffness of their substrate. Science. 2005;310:1139–43.
16. Engler AJ, Sen S, Sweeney HL, Discher DE. Matrix elasticity directs stem cell lineage specification. Cell. 2006;126:677–89.
17. Shimomura S, Matsuno H, Tanaka K. Effect of mechanical instability of polymer scaffolds on cell adhesion. Langmuir. 2013;29:11087–92.
18. Shimomura S, Matsuno H, Sanada K, Tanaka K. Cell adhesion on glassy scaffolds with a different mechanical response. J Mater Chem B. 2017;5:714–9.
19. Matsuno H, Irie S, Hirata T, Matsuyama R, Oda Y, Masunaga H, et al. Heterogeneous adhesion of cells on polymer surfaces with underlying amorphous/crystalline phases. J Mater Chem B. 2018;6:903–7.
20. Shimomura S, Matsuno H, Kinoshita Y, Fujimura S, Tanaka K. Cellular behaviors on polymeric scaffolds with 2D-patterned mechanical properties. Polym J. 2018;50:737–43.
21. Iwamatsu K, Uto K, Takeuchi Y, Hoshi T, Aoyagi T. Preparation of temperature-responsive, cationized, poly(ε-caprolactone)-based, cross-linked materials by a macromonomer design and positive charge control on the surface. Polym J. 2018;50:447–54.
22. Tanaka K, Fujii Y, Atarashi H, Akabori K, Hino M, Nagamura T. Nonsolvents cause swelling at the interface with poly(methyl methacrylate) films. Langmuir. 2008;24:296–301.
23. Atarashi H, Hirai T, Hori K, Hino M, Morita H, Serizawa T, et al. Uptake of water in non-annealed poly(methyl methacrylate) thin films. RSC Adv. 2013;3:3516–9.
24. Tateishi Y, Kai N, Noguchi H, Uosaki K, Nagamura T, Tanaka K. Local conformation of poly(methyl methacrylate) at nitrogen and water interfaces. Polym Chem. 2010;1:303–11.
25. Hirata T, Matsuno H, Kawaguchi D, Yamada NL, Tanaka M, Tanaka K. Effect of interfacial structure on bioinert properties of poly(2-methoxyethyl acrylate)/poly(methyl methacrylate) blend films in water. Phys Chem Chem Phys. 2015;17:17399–405.
26. Matsuno H, Tsukamoto R, Shimomura S, Hirai T, Oda Y, Tanaka K. Platelet-adhesion behavior synchronized with surface rearrangement in a film of poly(methyl methacrylate) terminated with elemental blocks. Polym J. 2016;48:413–9.
27. Yamamoto K, Hirai T, Oda Y, Kawaguchi D, Matsuno H, Tanaka K. A polymer interfacial modifier synthesized by living anionic polymerization: incorporation of inorganic blocks to chain ends. Macromol Chem Phys. 2017;218:1600473.
28. Fréchet JMJ. Functional polymers and dendrimers: reactivity, molecular architecture, and interfacial energy. Science. 1994;263: 1710–5.
29. Voit BI, Lederer A. Hyperbranched and highly branched polymer architectures – synthetic strategies and major characterization aspects. Chem Rev. 2009;109:5924–73.
30. Bandyopadhyay A, Sengupta S, Das T. Hyperbranched polymers for biomedical applications, springer series on polymer and composite materials. Springer: Singapore; 2017.
31. Navarro L, Ceaglio N, Rintoul I. Structure and properties of biocompatible poly(glycerol adipate) elastomers modified with ethylene glycol. Polym J. 2017;49:625–32.
32. Yang Y, Cai Z, Huang Z, Tang X, Zhang X. Antimicrobial cationic polymers: from structural design to functional control. Polym J. 2018;50:33–44.
33. Yuasa S, Imoto H, Naka K. Synthesis and properties of hyperbranched polymers by polymerization of an AB3-type incompletely condensed cage silsesquioxane (IC-POSS) monomer. Polym J. 2018;50:879–87.
34. Atarashi H, Ariura F, Akabori K, Ozawa M, Tanaka K, Nagamura T. Interfacial segregation of hyper-branched polystyrene in mixture of linear component. Trans Mater Res Soc Jpn. 2007;32: 231–4.
35. Hirai T, Liu H, Ohta Y, Yokozawa T, Tanaka K. Surface segregation of well-defined *N*-substituted hyperbranched polyamides in liner polymer matrix. Chem Lett. 2011;40:366–7.
36. Haraguchi M, Hirai T, Ozawa M, Miyaji K, Tanaka K. Hydrophobic acrylic hard coating by surface segregation of hyperbranched polymers. Appl Surf Sci. 2013;266:235–8.
37. Tanaka K, Hirai T, Shimafuji K, Haraguchi M, Matsuyama M. PCT International Applications. WO 2013191294*A1* (2013).
38. Totani M, Liu L, Matsuno H, Tanaka K. Design of a star-like hyperbranched polymer having hydrophilic arms for anti-biofouling coating. J Mater Chem B. 2019;7:1045–9.
39. Akdemir ZS, Kayaman-Apohan N, Kahraman MV, Kuruca SE, Gungor A, Karadenizli S. Preparation of biocompatible, UV-cured fumarated poly(ether-ester)-based tissue-engineering hydrogels. J Biomater Sci Polym Ed. 2011;22:857–72.
40. Das B, Chattopadhyay P, Mandal M, Voit B, Karak N. Bio-based biodegradable and biocompatible hyperbranched polyurethane: a scaffold for tissue engineering. Macromol Biosci. 2013;13: 126–39.
41. Dong Y, Saeed AO, Hassan W, Keigher C, Zheng Y, Tai H, et al. "One-step" preparation of thiol-ene clickable PEG-based

thermoresponsive hyperbranched copolymer for *in situ* crosslinking hybrid hydrogel. Macromol Rapid Commun. 2012;33:120–6.
42. Kennedy R, Hassan WU, Tochwin A, Zhao T, Dong Y, Wang Q, et al. *In situ* formed hybrid hydrogels from peg based multi-functional hyperbranched copolymers: a RAFT approach. Polym Chem. 2014;5:1838–42.
43. Brandrup J, Immergut EH, Grulke EA. Polymer handbook, 4th ed., Wiley-Interscience: Hoboken, NJ; 2003.
44. Kassis CM, Steehler JK, Betts DE, Guan Z, Romack TJ, DeSimone JM, et al. XPS studies of fluorinated acrylate polymers and block copolymers with polystyrene. Macromolecules. 1996;29: 3247–54.
45. Hynes, RO. Fibronectins, springer series in molecular and cell biology. Springer-Verlag: New York, NY; 1990.
46. Curtis SG, Forrester JV, McInnes C, Lawrie F. Adhesion of cells to polystyrene surfaces. J Cell Biol. 1983;97:1500–6.
47. Tamada Y, Ikada Y. Cell adhesion to plasma-treated polymer surfaces. Polymer. 1993;34:2208–12.
48. Lerman MJ, Lembong J, Muramoto S, Gillen G, Fisher JP. The evolution of polystyrene as a cell culture material. Tissue Eng B. 2018;24:359–72.
49. Leclerc E, David B, Griscom L, Lepioufle B, Fujii T, Layrolle P, et al. Study of osteoblastic cells in a microfluidic environment. Biomaterials. 2006;27:586–95.